Universiteit Leiden
The Netherlands

The glycocalyx: a diagnostic and therapeutic target in cardiometabolic diseases

Velden, A.I.M. van der

Citation

Velden, A. I. M. van der. (2024, September 3). *The glycocalyx: a diagnostic and therapeutic target in cardiometabolic diseases*. Retrieved from https://hdl.handle.net/1887/4039604

Version:	Publisher's Version
License:	Licence agreement concerning inclusion of doctoral thesis in the Institutional Repository of the University of Leiden
Downloaded from:	https://hdl.handle.net/1887/4039604

Note: To cite this publication please use the final published version (if applicable).

CHAPTER 6

Fasting mimicking diet in diabetic mice partially preserves glomerular endothelial glycocalyx coverage, without changing the diabetic metabolic environment

Anouk I.M. van der Velden
Angela Koudijs
Sander Kooijman
Rosalie G.J. Rietjens
Wendy M.P.J. Sol
M. Cristina Avramut
Gangqi Wang
Patrick C.N. Rensen
Ton J. Rabelink
Johan van der Vlag*
Bernard M. van den Berg*
***Share last authorship**

American Journal of Physiology
Renal Physiology
2024, 326(5): F681-F693

Abstract

Intermittent fasting has become of interest for its possible metabolic benefits and reduction of inflammation and oxidative damage, all of which play a role in pathophysiology of diabetic nephropathy. We tested in a streptozotocin (60mg/kg) induced diabetic ApoE-KO mouse model whether repeated fasting mimicking diet (FMD) prevents glomerular damage. Diabetic mice received 5 FMD cycles in 10 weeks and during cycles 1 and 5 caloric measurements were performed. After 10 weeks, glomerular endothelial morphology was determined together with albuminuria, urinary heparanase-1 (HPSE-1) activity, and spatial mass spectrometry imaging (MSI) to identify specific glomerular metabolic dysregulation. During FMD cycles, blood glucose levels dropped while a temporal metabolic switch was observed to increased fatty acid oxidation. Overall bodyweight at the end of the study was reduced together with albuminuria, although urine production was dramatically increased without affecting urinary HPSE-1 activity. Weight loss consisted of the loss of lean mass and water, not the loss of fat mass. While capillary loop morphology and endothelial glycocalyx heparan sulfate contents were preserved, hyaluronan surface expression was reduced together with the presence of UDP-glucuronic acid. MSI further revealed reduced protein catabolic breakdown products and increased oxidative stress, not different then diabetic mice. In conclusion, although FMD preserves partially glomerular endothelial glycocalyx, loss of lean mass and increased glomerular oxidative stress argue whether such diet regimes are safe in patients with diabetes.

Introduction

Over the years, intermittent fasting has become a topic of interest in the dietary field, since this type of fasting not only has metabolic benefits, but is also able to induce cellular changes that affect inflammation and oxidative damage [1, 2]. These changes would consequently enhance cellular protection and optimize energy metabolism [2]. The newly introduced periodic fasting-mimicking diet (FMD) regime that induces such beneficial cellular effects, in addition, should be easier to keep up compared to other types of fasting. During the fasting periods, when glucose and glycogen storages are depleted, metabolism switches to the utilization of ketones and fatty acids as the main source of energy. Previous fasting studies showed the beneficial effects of such a diet on endothelial function [3] and reduced body mass index, blood pressure, fasting glucose, total and low-density cholesterol, C-reactive protein and IGF-1 levels in generally healthy participants [4]. Furthermore, FMD in diabetes was effective in experimental type 1 and type 2 mouse models, where diabetic characteristics were ameliorated as blood glucose levels normalized and insulin sensitivity improved, mainly directed by regeneration of the pancreatic beta cells [5, 6].

The effect of FMD specifically on the diabetic kidney has not been studied yet. Endothelial dysfunction is considered the first marker of vascular complications, which can progress to structural microvascular changes and eventually results in irreversible vascular damage [7-9]. Diabetes induced endothelial activation is characterized by a pro-inflammatory and pro-thrombotic phenotype, loss of vascular integrity, and changes in endothelial glycocalyx composition [10]. Prolonged endothelial activation ultimately leads to endothelial dysfunction and upregulation of glycocalyx degrading enzymes such as heparanase-1 (HPSE-1) [11]. As fasting is accompanied by reprogramming of cellular processes towards survival and resilience, we aimed to investigate whether a recurrent 4-day FMD regime has the ability to preserve glomerular capillary morphology and glomerular endothelial surface glycocalyx in a diabetic model. For this, we used a streptozotocin-induced diabetic mice, known to induce impairment of the glomerular glycocalyx [12, 13]. To determine the possible metabolic changes upon FMD, we placed the animals in metabolism cages and at the end of the experiment determined glomerular metabolite changes using spatial mass-spectrometry [14].

Materials and methods

Diabetic ApoE-KO mouse model

Six-week-old male B6.129P2-*Apoe*^{tm1Unc}/J mice (ApoE-KO; The Jackson Laboratory, Bar Harbor, ME) were rendered diabetic through intraperitoneal injections of 60mg/kg

streptozotocin (STZ; Sigma-Aldrich, St. Louis, MO) for 5 consecutive days, as described before [12] (figure 1A). ApoE-KO mice were injected with citrate buffer alone (control) and to reduce the overall discomfort level we reduced the amount of handlings during the experimental procedure we only used these non-diabetic mice were used for baseline measurements. All mice had free access to standard rodent diet (NC; Ssniff Spezialdiäten GmbH, Soest, Germany). At week 8, diabetic mice were fed cholesterol enriched (0.15%) chow until the end of the study. At week 11, diabetic mice manifested with hyperglycemia, weight loss, polyuria and albuminuria (figure 2A,B) which were then used in the study. At week 12, six weeks after induction of diabetes, diabetic mice were randomized into the diabetic group (Diabetic) fed cholesterol enriched (0.15%) chow for 10 weeks or into a diabetic group that received a 4 day fasting mimicking diet (FMD) that was repeated 5 times in 10 weeks. In between the diet interventions, FMD mice were fed cholesterol enriched (0.15%) chow. Animal experiments were approved by the Ethical Committee on Animal Care and Experimentation at the Leiden University Medical Center (permit no. AVD1160020172926). All work with animals was performed in compliance with the Dutch government's guidelines.

Blood glucose concentrations were measured with an Accu-check glucose meter (Roche, Basel, Switzerland). When glucose concentrations exceeded 20 mmol/L, mice were treated with 1–2 units insulin (Lantus, Aventis Pharmaceuticals, Bridgewater, NJ, US) up to three times per week (supplemental figure S1D, E). Sixteen weeks after STZ injections, at 22 weeks of age, mice were sacrificed.

Mouse fasting mimicking diet

The FMD used in the study was provided by the Longo group as a gift and consisted of a 4-day regimen similar to the diet used by Brandhorst *et al.* [1]. Day 1 of the diet contained 7.67 kJ/g and consisted of a mix of various low-calorie broth powders, a vegetable medley powder, extra virgin olive oil, and essential fatty acids; day 2–4 diet contained 1.48 kJ/g and consisted of low-calorie broth powders and glycerol. The diet ingredients were thoroughly mixed and then blended together with hydrogel (ClearH_2O, Westbrook, ME, USA).

Caloric measurements

In weeks 12 and 20, control-, diabetic- and FMD mice were placed in metabolism cages (Sable Systems Europe GmbH, Berlin, Germany) for 4 days to measure food intake, oxygen ($V\cdot_{O_2}$) consumption, carbon dioxide ($V\cdot_{CO_2}$) production and ambulatory physical activity (semi quantitative by beam breaks). Followed by Echo-MRI (EchoMRI LLC, Houston, TX, USA) to measure body composition (lean-, fat mass, total- and free water). Based on these values, we calculated the respiratory exchange ratio (RER, the ratio of carbon dioxide produced by the body to oxygen consumed by the body), energy expenditure, carbohydrate and fat oxidation rates to monitor possible metabolic changes. In addition,

from the Echo-MRI data muscle mass and %muscle mass were calculated as followed, since lean mass measurements are the total of muscle mass + (total water- free water), muscle mass was calculated by lean mass - (total water- free water), %muscle mass was calculated as muscle mass/(lean mass + fat mass) x 100.

Urine collection and analysis

Mice were weighted before and after residing in a metabolic cage (Tecniplast S.p.a, Buguggiate, Italy) and water- and food intake and urine were collected. After acclimatization, 14 h-urine was collected at week 11, 17 and 21. Urine samples were centrifuged to remove debris and stored at -20°C. Urinary albumin concentrations were quantified with an enzyme-linked immunosorbent assay (ELISA; Bethyl Laboratories, Inc. Montgomery, TX, USA) and creatinine concentrations were quantified by the Jaffe´ method using 0.13% picric acid and a creatinine standard set (Sigma-Aldrich, Merck Life Science NV, Amsterdam, The Netherlands). Urinary MCP-1 and KIM-1 (kidney injury molecule-1) were measured with a commercially available immunoassay according to the manufacturer protocol (MJE00B and MKM100, resp.: R&D Systems Europe, Ltd., Abingdon, UK). Urinary heparanase activity was measured with a commercially available ELISA assay (Takara Bio Inc., Shiga, Japan). For this, urine samples were run through Zeba™ Spin Desalting Columns (ThermoFisher Inc., Waltham, MA, USA) for removal of salts and other small molecules (<1000 MW).

Glomerular endothelial glycocalyx coverage

Glycocalyx coverage was determined using fluorescently labelled lectin *Lycopersicon esculentum* (LEA-FITC) and the N terminus rat neurocan construct of the hyaluronan-specific neurocan-dsRed (Ncan-dsRed) construct, as described previously [15, 16]. In short, overnight PFA fixed tissue was subsequently sectioned in 100µm thick slices with a Leica VT1000S vibratome (n = 3/group) and submerged in HBSS (Life Technologies Europe BV, Bleiswijk, The Netherlands) containing 0.5% BSA, 5 mmol/L HEPES, and 0.03 mmol/L EDTA (HBSS-BSA). Slices were incubated with 10 mg/mL LEA-FITC or Ncan-dsRed [16] to visualize the glycocalyx, together with 5 mg/mL monoclonal mouse anti-mouse CD31 antibody (Santa Cruz Biotechnology, Santa Cruz, CA) to identify the endothelial cell membrane, overnight at 4°C on a shaker (in dark). After 3 washes with HBSS-BSA slices were incubated for 2 h with 10mg/mL Alexa Fluor-568, or AF488–conjugated goat anti-mouse IgG (Molecular Probes, Grand Island, NY) and Hoechst 33528 (Sigma-Aldrich, 1:1000) at 4°C on a shaker (in dark). Slices in HBSS-BSA were fixated between glass slide and coverslip in mounting medium and imaged on a LEICA TCS SP8 X WLL microscope (Leica, Rijswijk, The Netherlands) and a 40x objective (HC PL APO CS2 40x/1.30 OIL, Leica). Sequential 16-bit confocal images (xyz dimensions, 0.142 x 0.142 x 0.3 µm) were recorded using LAS-X Image software (Leica). The amount of endothelial glycocalyx was quantified in using 5 lines of interest in 3-4 glomeruli per kidney by calculating the distance from the peak of the

CD31 signal to the half-width of the luminal LEA-FITC or Ncan-dsRed signal along a line of interest, using intensity profiles (ImageJ), as described previously [16].

Tissue preparation and histology

Mice were anesthetized by isoflurane inhalation and perfused via the left ventricle with HEPES-buffered salt solution containing 0.5% bovine serum albumin and 5 U/mL heparin to remove blood. After removal of the kidney capsules, the left kidney was placed in 2% PFA in PBS overnight at 4°C, followed by paraffin embedding for periodic acid-Schiff (PAS), methenamine silver-periodic acid-Schiff (MPAS) or immunofluorescence staining. The left kidney of a subset of mice (n = 3/group) was perfused with 5mL Hanks-buffered salt solution (HBSS, Gibco) containing 0.5% BSA (Sigma, A7030, essentially globulin free) and 5U/mL heparin at 2mL/minute to remove blood, followed by 2mL of cationic ferritin (horse spleen, 2.5mg/mL, Electron Microscopy Sciences, Fort Washington, PA) in HBSS at 2mL/minute. The kidney was excised, its capsule removed, and stored in fixative (1.5% glutaraldehyde and 1% paraformaldehyde (PFA) (both from Electron Microscopy Sciences, Hatfield, PA) in 0.1M sodium-cacodylate buffered solution, pH 7.4) overnight at 4°C for further processing for transmission electron microscopy (TEM).

TEM cationic ferritin determination

Cationic ferritin perfused tissue, stored in fixative, 1.5% GA and 1% PFA in 0.1M sodium-cacodylate buffered solution, was subsequently sectioned in 180µm thick slices with a Leica VT1000S vibratome, rinsed 2x with 0.1M sodium cacodylate-buffered solution, and post-fixated for 1hr with 1% osmium tetroxide (Electron Microscopy Sciences) and 1.5% potassium ferrocyanide in demineralized water [15, 16]. Samples were further washed, dehydrated in ethanol, infiltrated with a mixture of epon LX-112 and propylene oxide (1:1) for 1 hr, followed by pure epon for 2hrs, embedded in epon mounted in BEEM capsules (Agar Scientific, Essex, United Kingdom) and polymerized for 48hrs at 60°C. 100nm Thick sections were cut using a diamond knife (Diatome, Biel, Switzerland), collected on single slot copper grids covered with formvar film and carbon layer, and then stained with 7% uranyl acetate in demineralized water for 20 minutes, followed by Reynold's lead citrate for 10 minutes. Data was collected at an acceleration voltage of 120kV on a Tecnai G2 Spirit BioTWIN transmission electron microscope (TEM), equipped with an FEI 4k Eagle CCD camera. Virtual slides were acquired with 18,500x magnification at the detector plane, corresponding to a 1.2nm pixel size at the specimen level. Representative capillary sections of each recorded glomerulus (n = 1/group) from virtual slides were selected for display as a high resolution image.

Glomerular tissue metabolomics

Frozen renal tissue sections (stored at -80°C) of a subset of mice (n= 4/group) were embedded in deionized water (MQ) and sections of 10 µm thickness were cryosectioned

using a Cryostar NX70 cryostat (Thermo Fisher Scientific, MA, USA) at -20 °C. The sections were thaw-mounted onto indium-tin-oxide (ITO)-coated glass slides (VisionTek Systems Ltd., Chester, UK). Mounted sections were placed in a vacuum freeze-dryer for 15 minutes prior to matrix application. After drying, *N*-(1-naphthyl) ethylenediamine dihydrochloride (NEDC) (Sigma-Aldrich, UK) MALDI-matrix solution of 7 mg/mL in methanol/acetonitrile/deionized water (70, 25, 5 %v/v/v) was applied using a SunCollect sprayer (SunChrom GmbH, Friedrichsdorf, Germany). A total of 17 matrix layers were applied with the following flowrates: layer 1-3 at 5 µL/min, layer 4-6 at 10 µL/min, layer 7-9 at 15 µL/min and 10-17 at 20 µL/min (speed *x*, medium 1; speed *y*, medium 1; *z* position, 35). The ITO glass slide containing the slices of all three groups were scanned using matrix-assisted laser desorption/ionization time-of-flight mass spectrometry imaging (MALDI-TOF-MSI) with the RapifleX MALDI-TOF/TOF system (Bruker Daltonics GmbH, Bremen, Germany). Negative ion-mode mass spectra were acquired at a pixel size of 20 × 20 μm^2 in a mass range from *m/z* 80-1000 in reflectron mode. Prior to analysis the instrument was calibrated using red phosphorus. Spectra were acquired with 200 laser shots per pixel at a laser repetition rate of 10 kHz. Data acquisition was performed using flexControl (Version 4.0, Bruker Daltonics, Germany) and visualizations were obtained from flexImaging 5.0 (Bruker Daltonics). MALDI-FTICR-MSI was performed on a 12T solariX FTICR mass spectrometer (Bruker Daltonics GmbH, Bremen, Germany) in negative-ion mode, using 30 laser shots and 50 µm pixel size. Prior to analysis the instrument was calibrated using red phosphorus. The spectra were recorded in a *m/z* range of 100-1000 with a 512k data point transient and transient length of 0.1049 seconds. Data acquisition was performed using ftmsControl (Version 2.1.0, Bruker Daltonics), and visualizations were obtained from flexImaging 5.0 (Bruker Daltonics). The *m/z* features present in both MALDI-TOF-MSI and MALDI-FTICR-MSI datasets, and which had similar tissue distributions, were further used for identity assignment of metabolites and lipid species. The *m/z* values from MALDI-FTICR-MSI were imported into the Human Metabolome Database[17] (https://hmdb.ca/) and annotated for metabolites and lipids species with an error < ±10 ppm. For the small molecules detected only in MALDI-TOF, the *m/z* values from MALDI-TOF were imported into the Human Metabolome Database (https://hmdb.ca/) and annotated for metabolites with an error < ±20 ppm. MSI data of the glomerular regions of interest were exported and processed in SCiLS Lab 2016b (SCiLS GmbH). All MALDI-TOF/TOF-MSI data was normalized to the total ion count (TIC). The peaks from the skyline/basepeak spectrum with a signal-to-noise-ratio higher than 3 were selected and all matrix peaks were excluded. A total of 389 *m/z*-features were selected by peak intensities. For specific spatial analysis of the glomerular areas post MALDI-MSI immunofluorescent staining was performed using the endothelial specific lectin from *Bandeiraea simplicifolia* (BS-I-TRITC, 1:200, Sigma, L5264) as described previously [14]. The differential expression of metabolites and lipids between groups were analyzed using both a two-way analysis of variance (ANOVA) test followed with Tukey's post-hoc test and classical univariate ROC curve analysis from the

MetaboAnalyst online version (https://www.metaboanalyst.ca/) [18]. A cutoff (AUC > 0.7 and p < 0.01) was taken for further pathway analysis using Reactome database (https://reactome.org/) [19] and lipid ontology analysis using LION/web (http://www.lipidontology.com/) [20]. Heatmaps were produced using the R pheatmap package based on the average value of metabolites.

Statistical analysis

Data are presented as means with standard deviation (SD). Differences in experiments were determined using analysis of variance and post hoc analyses with Tukey's multiple comparison test. Comparison of expression between two different groups was evaluated using a t-test and changes overtime between groups using simple linear regression. Statistical analyses were performed using GraphPad Prism version 8 (Graphpad Inc., La Jolla, CA, USA). A significance level of 0.05 was considered statistically significant.

Results

Study setup diabetic ApoE-KO mice

Throughout the 10-week intervention period, body weight dropped during the FMD cycles but increased again in the refeeding period (figure 1B). Simple linear regression comparison of body weight gain, in weeks excluding FMD cycles, revealed a clear significant (p = 0.0089) change in slopes between diabetic and FMD mice (figure 1C), revealing an overall reduction in total body weight in mice subjected to repeated FMD compared to diabetic mice. Pilot experiments revealed that STZ-induced diabetes in the apoE-KO mouse model resulted in increasing blood glucose levels even above detection which in itself already induced a full body metabolic switch to predominant lipid oxidation were predominantly lipids over carbohydrates are used for energy consumption (comparable to

Figure 1. Design of mouse study and baseline characteristics. (A) Schematic representation of the mouse study. Mice were rendered diabetic using streptozotocin (STZ), controls received citrate buffer, at week 6. From week 8 until end of the experiments diabetic were fed cholesterol enriched chow while the fasting mimicking diet intervention group were replaced on this diet for 5 times which lasted 5 days each cycle. At various intervals urine was collected or mice were housed in metabolism cages for 72hrs each time. *Abbreviations: STZ = streptozotocin, 0.15%CC = 0.15% cholesterol enriched normal chow, MC = metabolism cage, UC = urine collection. X, endpoint.* **(B)** Weekly average body weights during experimental intervention period with fasting mimicking diet (FMD). **(C)** Simple linear regression comparison (slope) in body weights, excluding FMD cycles, between diabetic and FMD mice. Averaged weekly **(D)** blood glucose levels and **(E)** insulin administration to maintain preferred blood glucose levels (upper two dashed lines in **D**). **(D)** Lower lines represent mean ± standard deviation blood glucose levels of control apoE-KO mice. Differences in trend between groups were assessed by simple linear regression.

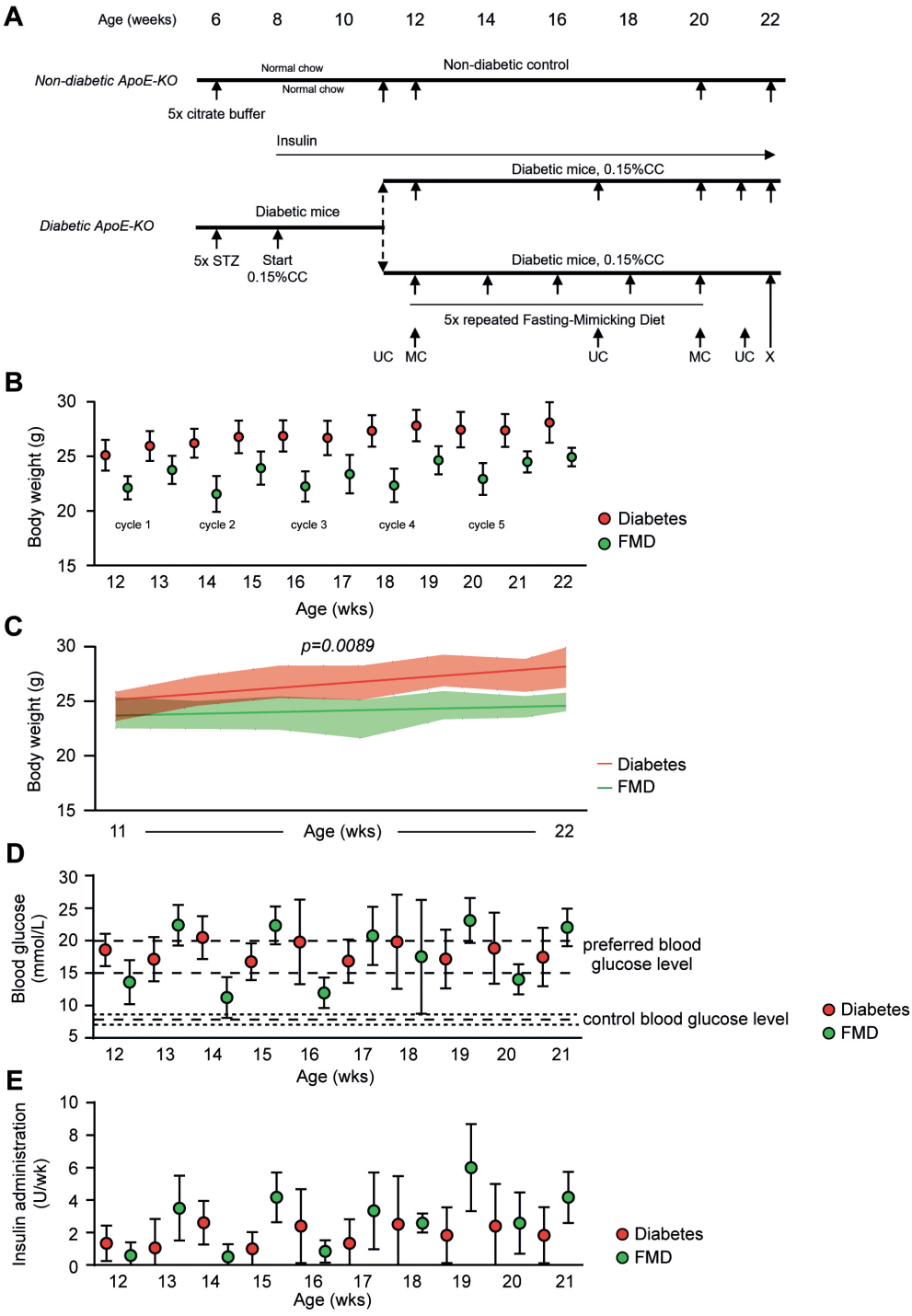
A
Age (weeks)
6
8
10
12
14
16
18
20
22
Non-diabetic ApoE-KO
Normal chow
Normal chow
Non-diabetic control
5x citrate buffer
Insulin
Diabetic mice, 0.15%CC
Diabetic ApoE-KO
Diabetic mice
5x STZ
Start 0.15%CC
Diabetic mice, 0.15%CC
5x repeated Fasting-Mimicking Diet
UC
MC
UC
MC
UC
X
B
Body weight (g)
cycle 1
cycle 2
cycle 3
cycle 4
cycle 5
Age (wks)
Diabetes
FMD
C
p=0.0089
Body weight (g)
Age (wks)
Diabetes
FMD
D
Blood glucose (mmol/L)
preferred blood glucose level
control blood glucose level
Age (wks)
Diabetes
FMD
E
Insulin administration (U/wk)
Age (wks)
Diabetes
FMD

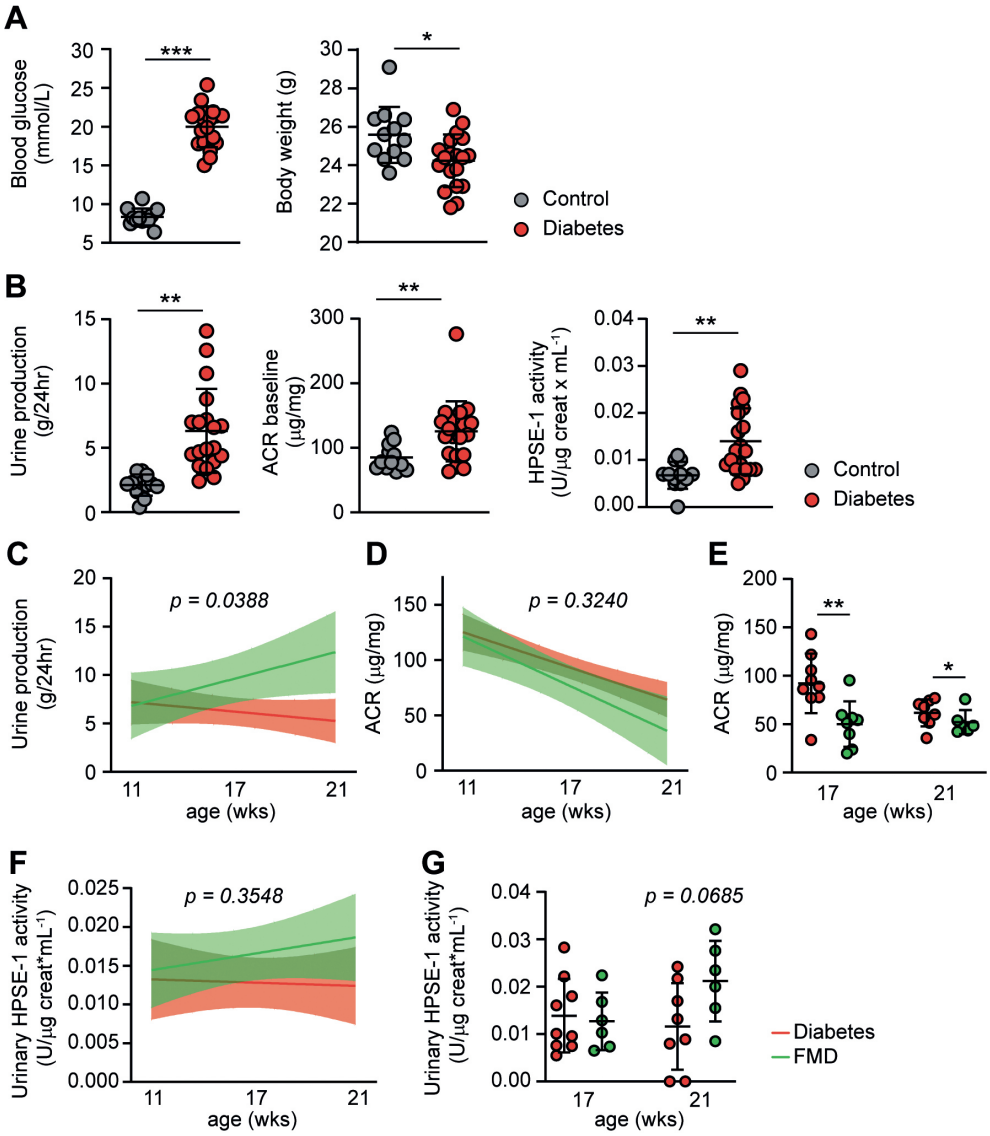

Figure 2. Blood glucose and urine measurements. (A) Blood glucose and body weight, and **(B)** urine production, albumin:creatinine ratio (ACR) and urinary heparanase 1 (HPSE-1) activity of control and diabetic mice at week 11, before randomization of diabetic mice in diabetic and fasting mimicking diet (FMD) groups. **(C)** Trends in urine production, and **(D)** albumin-to-creatinine ratio (ACR) in diabetic- (n = 8-9) and FMD (n = 6-8) mice over time (week 11-, 17- and 21). **(E)** 24-hour urine ACR concentrations at weeks 17 (n = 9 vs. n = 8) and 21 (n = 8 vs. n = 6) in diabetic and FMD mice, respectively. **(F)** Trends in urinary HPSE-1 activity in diabetes and FMD mice over time and **(H)** urinary HPSE-1 activity at week 17 (n = 9 vs. n = 6) and 21 (n = 8 vs. n = 6) in diabetic and FMD mice, respectively. Values are given as mean with standard deviation. Differences between groups were assessed by unpaired two-tailed t-test: *$P < 0.05$, **$P < 0.01$. ***$P < 0.001$. Differences in trend between groups were assessed by simple linear regression.

FMD group shown below, data not shown). Therefore, we kept the weekly average blood levels around 15-20 mmol/L as much as possible administration of insulin (figure 1D,E), to prevent such a preliminary shift to lipid usage for energy metabolism. Occasional insulin injections have been given throughout the entire experimental procedure with higher amounts in particular in the FMD group (figure 1D).

FMD reduces albuminuria

Before the intervention, at week 11, 5 weeks after STZ induction, diabetic mice manifested with hyperglycemia, weight loss, polyuria, albuminuria and increased urinary HPSE-1 activity levels (figure 1A,B). After these measurements, diabetic mice were randomized into a diabetic group fed cholesterol enriched (0.15%) chow only for 10 weeks or FMD group given a 4 day fasting mimicking diet that was repeated 5 times in 10 weeks with cholesterol-enriched chow ad libitum in between the FMD cycles (Figure 1A). At week 22, one week after the last FMD cycle, urine production was significantly higher in the FMD group compared to the diabetic group (figure 2C). Although during the whole intervention period albumin creatine ratio (ACR) in both diabetes and FMD mice were reduced equally, significantly lower ACR levels in the FMD could be detected at week 17, one week after 3 FMD cycles, and at the end of the experiment at week 21 compared to the diabetic group (figures 2D,E). Urinary levels of the potent heparan sulfate degrading enzyme HPSE-1 were not significantly different when compared to urinary activity in diabetic mice (figures 2F,G). Furthermore, urinary kidney injury molecule-1 (KIM-1) and monocyte chemoattractant protein-1 (MCP-1) levels did not change or remained below threshold levels for detection in both diabetic groups when compared to control mice (data not shown).

FMD prevented glomerular capillary rarefaction

The hyperglycemia controlled diabetic mice, through insulin administration in combination with a cholesterol-enriched diet (0.15%) to induce vascular damage, resulted in minimal glomerular changes at the end of the experiment, as shown by PAS and MPAS stained examples (figure 3A). Although no changes in capillary surface area were observed, the number of capillaries per glomerulus, however, were significantly reduced in diabetic mice compared to controls (difference of -4.2 95% CI -5.8 - -2.6) (figure 3B, C). Diabetic mice after FMD cycles, on the contrary, showed comparable numbers of capillaries per glomerulus compared to control, suggesting that capillary loss and -ballooning were prevented in this group. No changes were observed in glomerular surface area (data not shown) and mesangial surface area (figure 3D).

FMD partially preserved the glomerular glycocalyx

We further investigated the minor glomerular changes through staining PFA fixed renal sections directly with the fluorescently labelled lectin (LEA-FITC) or hyaluronan (HA) specific probe Ncan-dsRed to test the effect of repeated FMD cycles on glomerular glycocalyx

presence (figure 3E and H). Diabetes reduced the glomerular intraluminal lectin thickness on the endothelium to 0.157 µm, compared to 0.272 µm in control mice (difference 0.117 µm 95% CI 0.059 - 0.175) and luminal surface coverage (figures 3E-G). In turn, repeated FMD cycles protected the glomerular endothelial glycocalyx with regard to the lectin stained structures, as the intraluminal thickness was 0.227 µm with a difference of 0.070 µm compared to the diabetes group (95% CI 0.012 - 0.128) and luminal coverage (figure 3E-G). However, staining for HA revealed no protection of surface presence after FMD cycles (figure 3H-J). Visualizing the glomerular endothelial glycocalyx through cationic ferritin coverage using transmission electron microscopy, confirmed protection of at least the charged glycosaminoglycans within the glomerular endothelial glycocalyx by repeated FMD cycles (figure 3K). Cationic ferritin was present at the luminal endothelial cell surface, within the fenestrae and underneath the endothelium of the control mice and FMD group. In contrast, disruption of cationic ferritin coverage alongside the luminal endothelial cell surface could be seen in the diabetic glomerulus (figure 3K, middle panel). These changes were without significant changes in glomerular basement membrane (GBM), podocyte foot process effacement or endothelial fenestration (data not shown).

Figure 3. Histological glomerular changes. **(A)** Representative images of periodic acid–Schiff (PAS, top) and (methenamine silver-periodic acid-Schiff (MPAS, bottom) stained glomeruli of control- (left), diabetic- (middle) and diabetic apoE-KO mice after fasting mimicking diet (FMD) interventions (right); scale bar, 50 µm. Quantification of **(B)** glomerular capillary surface area, **(C)** number of capillaries per glomerulus and **(D)** mesangial surface area. Analysis was performed on ± 50 glomeruli per sample in control- (grey, n = 9), diabetic- (red, n = 8) and diabetic apoE-KO mice after FMD interventions (green, n = 9). Values are given as mean with standard deviation (SD). **(E)** Representative images of direct glycocalyx staining using fluorescent labeled lectin *Lycopersicon esculentum* (LEA-FITC) and anti-CD31 antibodies for endothelial cell detection; scale bar 50µm. Quantification of **(F)** luminal glycocalyx (LEA) thickness and **(G)** luminal glycocalyx (LEA) coverage, assessed in a subset of n = 3 control- (grey), diabetic- (red) and diabetic apoE-KO mice after fasting mimicking diet (FMD) interventions (green). **(H)** Representative images of direct glycocalyx staining using fluorescent labeled neurocan (Ncan-dsRed) and anti-CD31 antibodies for endothelial cell detection; scale bar 50µm. Quantification of **(I)** luminal hyaluronan (Ncan-dsRed) thickness and **(J)** luminal hyaluronan (Ncan-dsRed) coverage, assessed in a subset of n = 3 control- (grey), diabetic- (red) and diabetic ApoE-KO mice after FMD intervention (green). **(K)** Representative transmission electron micrographs of cationic ferritin-stained glomerular endothelial surfaces in control-, diabetic- apoE-KO and diabetic apoE-KO after FMD intervention, scale bars 1µm. Values are given as mean with standard deviation. Differences between groups were assessed by ANOVA with Tukey's post-hoc test: *$P < 0.05$, **$P < 0.01$.

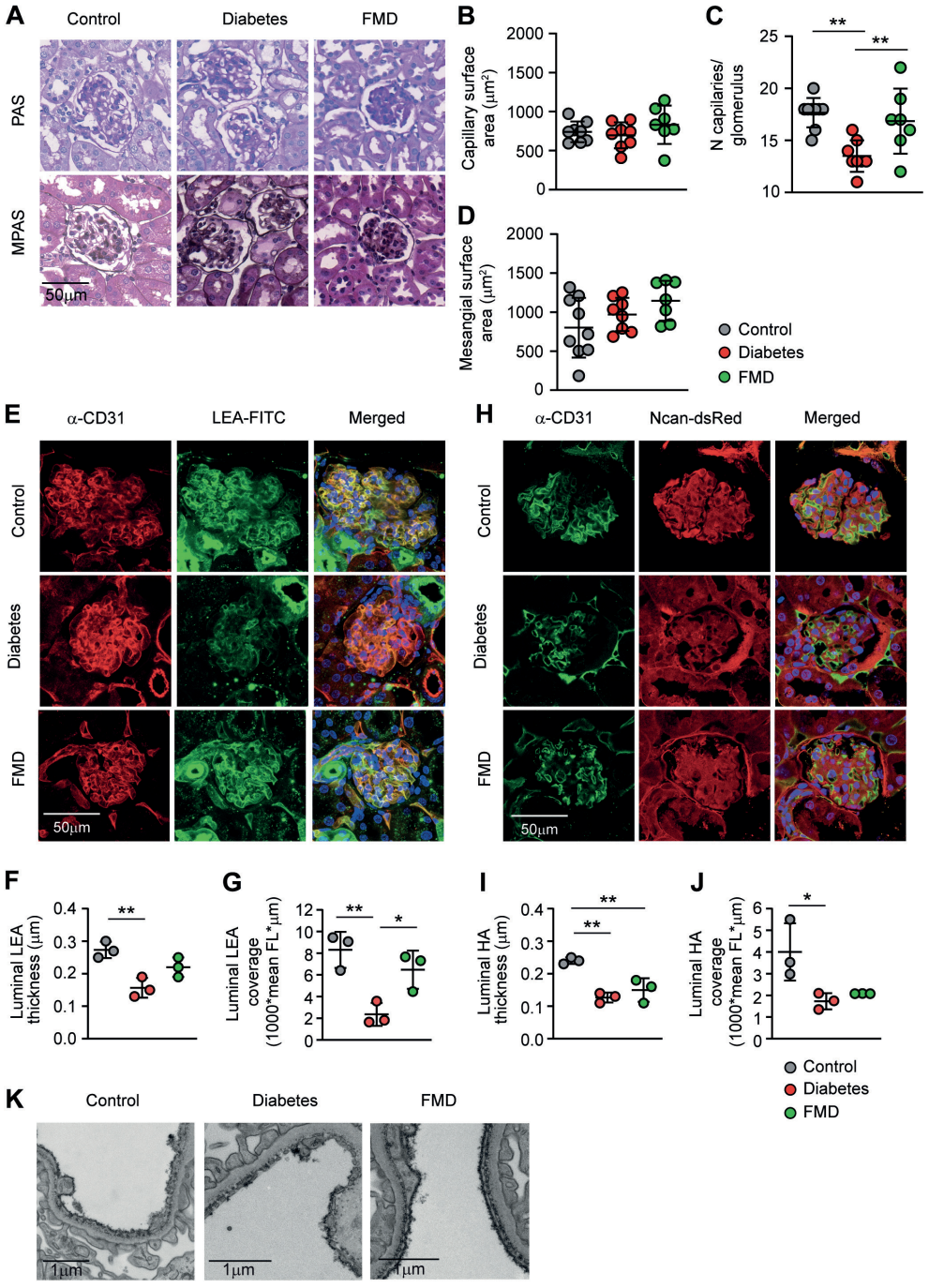
A
Control
Diabetes
FMD
PAS
MPAS
50µm
B
Capillary surface area (µm²)
2000
1500
1000
500
0
C
N capillaries/ glomerulus
25
20
15
10
**
**
D
Mesangial surface area (µm²)
2000
1500
1000
500
0
Control
Diabetes
FMD
E
α-CD31
LEA-FITC
Merged
Control
Diabetes
FMD
50µm
H
α-CD31
Ncan-dsRed
Merged
Control
Diabetes
FMD
50µm
F
Luminal LEA thickness (µm)
0.4
0.3
0.2
0.1
0.0
**
G
Luminal LEA coverage (1000*mean FL*µm)
12
10
8
6
4
2
0
**
*
I
Luminal HA thickness (µm)
0.4
0.3
0.2
0.1
0.0
**
**
J
Luminal HA coverage (1000*mean FL*µm)
6
5
4
3
2
1
0
*
Control
Diabetes
FMD
K
Control
Diabetes
FMD
1µm
1µm
1µm

FMD induced metabolic changes in diabetic ApoE-KO mice

During each 4-day FMD cycle, average body weight and glucose levels dropped but raised again as soon as the cycle was finished and animals were given cholesterol enriched food ad libitum (figure 4A, B). As revealed by the respiratory quotient ratio (RQ), defined as the volume of carbon dioxide released over the volume of oxygen absorbed during respiration, the reduced basal metabolic rate in diabetic mice indicated the use of more lipids over carbohydrates for energy consumption (figure 4C). During the FMD cycles, RQ dropped even further, indicating a full body metabolic switch to predominant lipid oxidation within each cycle. In addition, energy expenditure, reflecting animal movement, during the night and especially day cycle was increased during the last FMD cycle (figure 4D). These changes argue that these animals are more constantly searching for food. Additional Echo-MRI measurements revealed that the main component of weight loss during FMD cycles was loss of lean mass instead of fat mass (figure 4E). The major components of lean mass, total water and muscle mass, were both significantly reduced during the FMD cycle compared to the diabetic mice (figure 4F).

Figure 4. Effects of fasting mimicking diet (FMD) on metabolism and Echo-MRI body composure measurements. (A) Body weight- and **(B)** blood glucose level changes during each FMD cycle of mice in FMD group. **(C)** Respiratory quotient and **(D)** Energy expenditure at day (left) and night (right) during FMD cycles 1 (wk12) and 5 (wk20) in control-, diabetic and FMD mice. **(E)** Average total body mass, fat mass, and lean mass (muscle mass + total water – free water) changes as measured with Echo-MRI in diabetic and FMD groups directly after FMD cycles 1 and 5, respectively. **(F)** Total water measurements and calculated muscle mass (lean mass – (total water- free water)) and % muscle mass (muscle mass/ (lean mass +fat mass) x 100) of diabetic and FMD mice. Values are given as mean with standard deviation. Differences between groups were assessed in by ANOVA with Tukey's post-hoc test **(C**,**D),** or by unpaired t-test **(E**,**F)**: $*P < 0.05$, $**P < 0.01$. $***P < 0.001$.

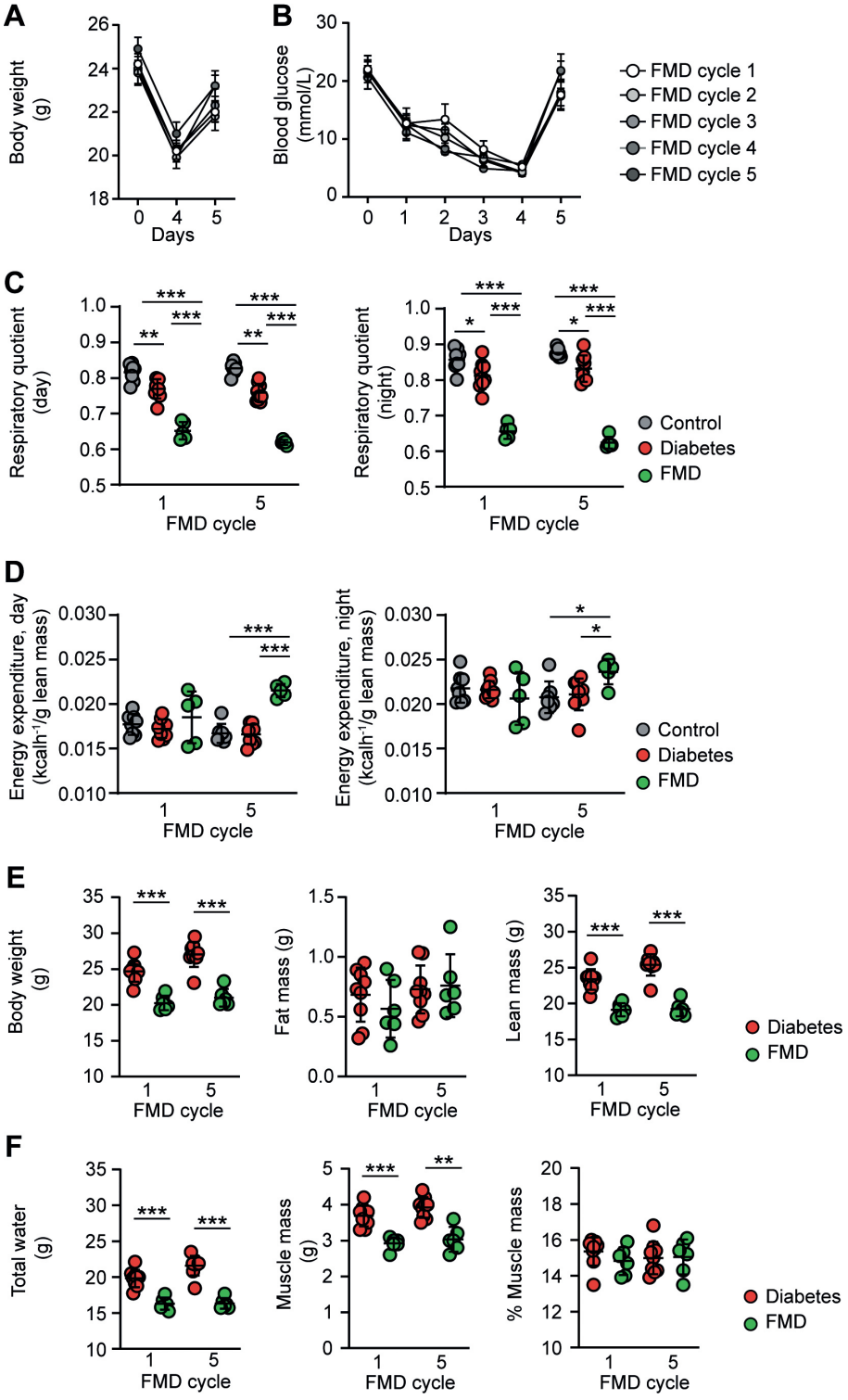
A
Body weight (g)
Days
B
Blood glucose (mmol/L)
Days
FMD cycle 1
FMD cycle 2
FMD cycle 3
FMD cycle 4
FMD cycle 5
C
Respiratory quotient (day)
Respiratory quotient (night)
FMD cycle
Control
Diabetes
FMD
D
Energy expenditure, day (kcalh-1/g lean mass)
Energy expenditure, night (kcalh-1/g lean mass)
FMD cycle
Control
Diabetes
FMD
E
Body weight (g)
Fat mass (g)
Lean mass (g)
FMD cycle
Diabetes
FMD
F
Total water (g)
Muscle mass (g)
% Muscle mass
FMD cycle
Diabetes
FMD

Glomerular metabolic changes upon FMD intervention

Following up on the metabolic changes observed in kidneys between control and diabetic mice [14], we now focused directly on changes in the glomerular areas between control, diabetic and FMD groups (figures 5A,B). Analysis of these three groups at the end of the experiment (week 22), 2 weeks after the final FMD intervention revealed that 31 of the 389 m/z features measured were significantly changed (figure 5C, supplemental table 1 and 2). Heatmap clustering revealed, horizontally, two major clusters; first the control group and a second cluster with both diabetes- and FMD groups. Vertical clusters revealed a large group with decreased metabolites and a small group with increased metabolite expression in the diabetes- and FMD group (figure 5C). Overall, compared to control mice, metabolite levels were all lower in the diabetes- and FMD group. The most pronounced change was observed in protein catabolism breakdown products, which were reduced in both the diabetes- and FMD group (figure 5C, supplemental table 1 and 2). Indications of increased oxidative stress were also observed with increased oxidized sphingolipid (m/z 737.5024; SM(d16:1/20:3(5Z,11Z,14Z)-O(8,9))) and ophthalmic acid, a reduced breakdown product of glutathione turnover. Finally, while the UDP-sugar metabolite UDP-GlcNAc did not change (control, 0.841 ± 0.141; diabetes, 0.819 ± 0.079; FMD, 0.769 ± 0.087), in diabetic mice UDP-GlcUA was significantly reduced ($P = 0.0295$) in diabetes and was not restored after repeated FMD cycles (figure 5C and supplemental table 2).

Figure 5. Glomerular metabolic changes. (A) Experimental workflow for in situ spatial MALDI- mass spectrometry imaging (MALDI-MSI) of control, diabetes, and diabetes mice after 5 cycles of fasting mimicking diet (FMD. **(B)** Experimental workflow for metabolic histologic analysis using fluorescent labeled *Bandeiraea simplicifolia* (BS-I) lectin staining to detect clustered glomerular endothelial cells which coincides with the metabolic m/z value of 566.33, and is used as specific glomerular marker in further analysis. **(C)** Heatmap showing the fractional contribution of significantly changed metabolites between control- (n = 4), diabetic (n = 4) and diabetic apoE-KO mice after fasting mimicking diet (FMD; n = 4), scaled by column. Representative metabolites are given in Annotation column. Differences between groups were assessed by two-way ANOVA with Tukey's post-hoc test. Cartoons were created with BioRender. Heatmap was produced using the R pheatmap package based on the average value of metabolites.

[§]Breakdown product of protein catabolism; [#]Not a natural metabolite, part of exposome; Blue font, metabolites in diabetes and FMD groups are both significantly different from control

A Spatial MALDI-mass spectrometry imaging

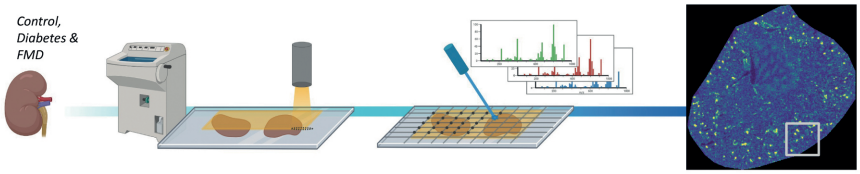

B Immuno fluorescent assisted cluster annotation

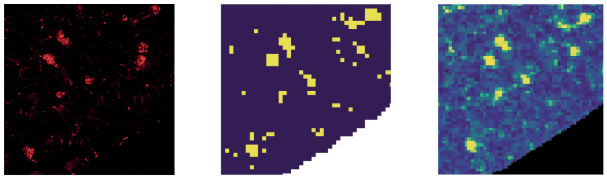

Bandeiraea simplicifolia (BS-I) lectin

Cluster

Metabolic marker *556.33 m/z*

C

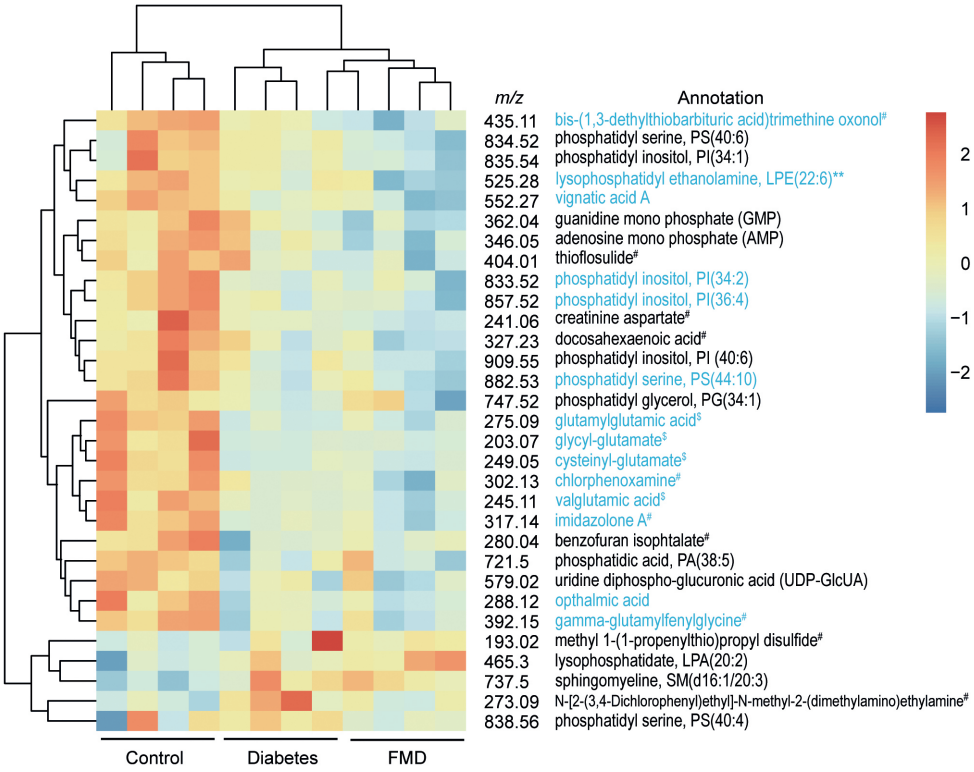

Discussion

In the present study, we observed that a periodic fasting mimicking diet in a diabetic mouse model reduced overall body weight, partially protected the glomerular endothelial surface glycocalyx layer and prevented glomerular capillary loop destruction. While during the FMD cycles fatty acid as a source of energy completely took over, loss of body mass was observed predominantly through loss of muscle mass instead of fat mass. At renal glomerular level, metabolite presence was not preserved in FMD mice when compared to diabetic and control mice. Here, presence of reduced fatty acids, protein breakdown products and UDP-GlcUA, key glycosaminoglycan substrate, were accompanied by increased oxidative stress.

After inducing diabetes, we observed that periodic FMD was able to protect the glomerular capillaries and its luminal glycocalyx, although with regard to the latter only a partial preservation was found as surface hyaluronan expression was not preserved. Although FMD could have a positive effect in inducing glycocalyx biosynthesis [16], the reduced amounts of one of its substrates, UDP-GlcUA, would prevent optimal hyaluronan synthesis by the main endothelial hyaluronan synthase 2 (HAS2) [21]. Meanwhile, other glycosaminoglycans such as heparan sulfate- and chondroitin sulfate glycosaminoglycans still could benefit, since these molecules are produced intracellularly within the Golgi-system, which exerts specific transporters to keep such substrates in high concentrations [22, 23]. Despite the reduced luminal hyaluronan presence, glomerular capillary rarefaction was prevented, although mice on the periodic FMD intervention in the continuous diabetic environment showed increasing urine production [16, 24].

During the FMD cycles, a metabolic switch to predominant lipid oxidation as energy source was induced, with an extensive reduction in blood glucose levels and body weight during the fasting days. This weight loss was dominantly caused by a reduction in lean mass, which mainly consisted of a significant loss of total water and muscle mass. Negative effects of fasting on muscle mass have been a big concern in fasting methods [25]. Several studies showed that adequate protein intake during weight loss regimes mitigate the loss of lean mass [26, 27]. Moreover, the FMD used in the current study has a very low amino acid/protein content [2, 6], which may enhance the risk of losing muscle mass during the fasting periods [28, 29]. In addition, a great reduction in total water was seen during the FMD cycles. In combination with increased urine production in the FMD mice, it suggest that the diet induces excessive water loss. Interestingly, during the overall 10 week period, the diabetic mice receiving the FMD showed additional weight loss on top of the reduced weight gain observed between diabetes- and control mice. With an overall raise in urine production and reduced muscle mass found, both fluid- and protein homeostasis

affected by the repeated FMD cycles could have exerted a lasting effect beyond the short periods of calorie restriction.

Following the overall total body metabolic assessment, we also used mass spectrometry imaging to specifically identify the glomerular metabolic status [14]. In a subset of control and diabetic kidney samples from our current study, we could determine diabetic related metabolic changes throughout the kidney, especially of small molecule metabolites and glycero(phoso)lipids in downstream nephron segments [14]. Although we observed in the total kidney samples a relative higher acetoacetate expression in both diabetes and FMD-treated mice compared to control (data not shown), focusing on glomeruli we observed in both diabetes- and FMD-treated mice overall lower metabolite levels, reduced protein catabolism breakdown products and increased oxidative stress markers. In particular, ophthalmic acid, a reduced breakdown product of glutathione turnover related to diminished glutathione synthesis, has been found in patients with uncontrolled diabetes [30, 31].

Our study has also several limitations. Despite the earlier positive effects observed in experimental type 1 and type 2 mouse models [5, 6], we did not observe changes in diabetes state nor an overall favourable effect on renal glomerular function. With regard to our STZ induced diabetes model we allocated only stable hyperglycaemic mice after 2 weeks to both the diabetic study arms. In our previous studies in the STZ-induced diabetes model on enriched cholesterol chow, we also did not observe recovery form the diabetes phenotype [12, 13]. Of note, in these previous studies we did observe a lasting increased ACR with increased mesangial surface area expansion and reduced nephrin expression, all for up to week 26. These overall changes coincided with loss of glomerular cationic ferritin and anti-HS antibody staining, intraluminal lectin staining (LEA), and increased glomerular HPSE and CTSL (cathepsin L) presence, all lacking in our current model. We observed that the diabetic model we used previously already displayed increased fatty-acid oxidation in diabetic mouse indiscernible from FMD. By administration of insulin to keep blood glucose levels within a preferred range, i.e. between 15-20mmol/L, we now could observe clear differences in metabolic state between diabetic and FMD mice. Unfortunately, this resulted in a very mild renal phenotype with only changes in glomerular capillary number and in glomerular endothelial glycocalyx coverage. Despite this limitation, our current model provided enough evidence to test for preservation of the glomerular endothelial cells and to observe the limited metabolic changes in the kidney in such a mild diabetic environment.

In conclusion, repeated FMD cycles in a STZ-induced diabetic mouse model, accompanied by periodic metabolic switches to overt lipid oxidation for energy, resulted in overall weight loss and prevented partially glomerular endothelial surface glycocalyx and capillary loss. However, weight loss was mainly found in lean and not fat mass and it did not

prevent glomerular metabolic changes as could be observed in diabetic mice. In diabetic mice after repeated FMD cycles, we still observed increased oxidative stress and reduced UDP-GlcA presence, possibly hampering hyaluronan synthesis.

References

1. Brandhorst, S., et al., *A Periodic Diet that Mimics Fasting Promotes Multi-System Regeneration, Enhanced Cognitive Performance, and Healthspan.* Cell Metab, 2015. **22**(1): p. 86-99.
2. Longo, V.D. and M.P. Mattson, *Fasting: molecular mechanisms and clinical applications.* Cell Metab, 2014. **19**(2): p. 181-92.
3. Yousefi, B., et al., *The effects of Ramadan fasting on endothelial function in patients with cardiovascular diseases.* Eur J Clin Nutr, 2014. **68**(7): p. 835-9.
4. Wei, M., et al., *Fasting-mimicking diet and markers/risk factors for aging, diabetes, cancer, and cardiovascular disease.* Sci Transl Med, 2017. **9**(377).
5. Wei, S., et al., *Intermittent administration of a fasting-mimicking diet intervenes in diabetes progression, restores beta cells and reconstructs gut microbiota in mice.* Nutr Metab (Lond), 2018. **15**: p. 80.
6. Cheng, C.W., et al., *Fasting-Mimicking Diet Promotes Ngn3-Driven beta-Cell Regeneration to Reverse Diabetes.* Cell, 2017. **168**(5): p. 775-788 e12.
7. Pomin, V.H., *Sulfated glycans in inflammation.* Eur J Med Chem, 2015. **92**: p. 353-69.
8. Zaporozhets, T. and N. Besednova, *Prospects for the therapeutic application of sulfated polysaccharides of brown algae in diseases of the cardiovascular system: review.* Pharm Biol, 2016. **54**(12): p. 3126-3135.
9. Schalkwijk, C.G. and C.D. Stehouwer, *Vascular complications in diabetes mellitus: the role of endothelial dysfunction.* Clin Sci (Lond), 2005. **109**(2): p. 143-59.
10. Dogne, S., B. Flamion, and N. Caron, *Endothelial Glycocalyx as a Shield Against Diabetic Vascular Complications: Involvement of Hyaluronan and Hyaluronidases.* Arterioscler Thromb Vasc Biol, 2018. **38**(7): p. 1427-1439.
11. Rabelink, T.J., et al., *Heparanase: roles in cell survival, extracellular matrix remodelling and the development of kidney disease.* Nat Rev Nephrol, 2017. **13**(4): p. 201-212.
12. Boels, M.G.S., et al., *Systemic Monocyte Chemotactic Protein-1 Inhibition Modifies Renal Macrophages and Restores Glomerular Endothelial Glycocalyx and Barrier Function in Diabetic Nephropathy.* Am J Pathol, 2017. **187**(11): p. 2430-2440.
13. Boels, M.G., et al., *Atrasentan Reduces Albuminuria by Restoring the Glomerular Endothelial Glycocalyx Barrier in Diabetic Nephropathy.* Diabetes, 2016. **65**(8): p. 2429-39.
14. Rietjens, R.G.J., et al., *Phosphatidylinositol metabolism of the renal proximal tubule S3 segment is disturbed in response to diabetes.* Sci Rep, 2023. **13**(1): p. 6261.
15. Dane, M.J., et al., *Glomerular endothelial surface layer acts as a barrier against albumin filtration.* Am J Pathol, 2013. **182**(5): p. 1532-40.
16. van den Berg, B.M., et al., *Glomerular Function and Structural Integrity Depend on Hyaluronan Synthesis by Glomerular Endothelium.* J Am Soc Nephrol, 2019. **30**(10): p. 1886-1897.
17. Wishart, D.S., et al., *HMDB 4.0: the human metabolome database for 2018.* Nucleic Acids Research, 2018. **46**(D1): p. D608-D617.
18. Pang, Z.Q., et al., *MetaboAnalystR 3.0: Toward an Optimized Workflow for Global Metabolomics.* Metabolites, 2020. **10**(5).
19. Jassal, B., et al., *The reactome pathway knowledgebase.* Nucleic Acids Research, 2020. **48**(D1): p. D498-D503.
20. Molenaar, M.R., et al., *LION/web: a web-based ontology enrichment tool for lipidomic data analysis.* Gigascience, 2019. **8**(6).
21. Wang, G., et al., *Shear Stress Regulation of Endothelial Glycocalyx Structure Is Determined by Glucobiosynthesis.* Arterioscler Thromb Vasc Biol, 2020. **40**(2): p. 350-364.

22. Hirschberg, C.B., P.W. Robbins, and C. Abeijon, *Transporters of nucleotide sugars, ATP, and nucleotide sulfate in the endoplasmic reticulum and Golgi apparatus.* Annu Rev Biochem, 1998. **67**: p. 49-69.
23. Caffaro, C.E. and C.B. Hirschberg, *Nucleotide sugar transporters of the Golgi apparatus: from basic science to diseases.* Acc Chem Res, 2006. **39**(11): p. 805-12.
24. Mauer, M., et al., *Glomerular structural-functional relationship models of diabetic nephropathy are robust in type 1 diabetic patients.* Nephrol Dial Transplant, 2015. **30**(6): p. 918-23.
25. Williamson, E. and D.R. Moore, *A Muscle-Centric Perspective on Intermittent Fasting: A Sub-optimal Dietary Strategy for Supporting Muscle Protein Remodeling and Muscle Mass?* Front Nutr, 2021. **8**: p. 640621.
26. Pasiakos, S.M., et al., *Effects of high-protein diets on fat-free mass and muscle protein synthesis following weight loss: a randomized controlled trial.* FASEB J, 2013. **27**(9): p. 3837-47.
27. Deibert, P., et al., *Weight loss without losing muscle mass in pre-obese and obese subjects induced by a high-soy-protein diet.* Int J Obes Relat Metab Disord, 2004. **28**(10): p. 1349-52.
28. Sartori, R., V. Romanello, and M. Sandri, *Mechanisms of muscle atrophy and hypertrophy: implications in health and disease.* Nat Commun, 2021. **12**(1): p. 330.
29. Saxton, R.A. and D.M. Sabatini, *mTOR Signaling in Growth, Metabolism, and Disease.* Cell, 2017. **169**(2): p. 361-371.
30. Sekhar, R.V., et al., *Glutathione synthesis is diminished in patients with uncontrolled diabetes and restored by dietary supplementation with cysteine and glycine.* Diabetes Care, 2011. **34**(1): p. 162-7.
31. Orlowski, M. and S. Wilk, *Synthesis of ophthalmic acid in liver and kidney in vivo.* Biochem J, 1978. **170**(2): p. 415-9.

Supplemental

Supplemental Table 1. List of significantly different metabolites in mouse kidney samples assigned by the mass measurements using both MALDI-TOF/TOF and MALDI-FTICR MS in negative ion mode.

calibrated m/z from MALDI-TOF/TOF	m/z from MALDI-FTICR	Ion	Annotation*	Theoretical m/z	Formula	ppm
193,0192	NA	[M-H]-	Methyl 1-(1-propenylthio)propyl disulfide	193,0185	C7H14S3	4
203,0676	**NA**	**[M-H]-**	**Glycyl-Glutamate/Alanylaspartic acid/Glutamylglycine/Aspartyl-Alanine/Alanyl-Aspartic acid/gamma-Glutamylglycine/L-beta-aspartyl-L-alanine**	**203,0673**	**C7H12N2O5**	**1**
241,0568	NA	[M-H]-	Creatinine aspartate	241,0578	C8H10N4O5	4
245,1134	**NA**	**[M-H]-**	**Valylglutamic acid/gamma-Glutamylvaline/Glutamylvaline/Leucyl-Aspartate/Isoleucyl-Aspartate/Aspartyl-Leucine/Aspartyl-Isoleucine/ L-beta-aspartyl-L-leucine**	**245,1143**	**C10H18N2O5**	**4**
249,0543	**NA**	**[M-H]-**	**Cysteinyl-Glutamate/Glutamylcysteine/N-gamma-Glutamylcysteine/ gamma-Glutamylcysteine**	**249,0551**	**C8H14N2O5S**	**3**
273,0936	NA	[M-H]-	N-(2-(3,4-Dichlorophenyl)ethyl)-N-methyl-2-(dimethylamino) ethylamine	273,0931	C13H20Cl2N2	2
275,0861	**275,0863**	**[M-H]-**	**Glutamylglutamic acid/D-gamma-Glutamyl-D-glutamic acid/ Thymidine glycol/gamma-Glutamylglutamic acid**	**275,0885**	**C10H16N2O7**	**8**
279,0369	NA	[M-H]-	**Benzofuran isophthalate	279,0299	C16H8O5	25
288,1197	**NA**	**[M-H]-**	**Ophthalmic acid**	**288,1201**	**C11H19N3O6**	**1**
302,1313	**NA**	**[M-H]-**	**Chlorphenoxamine/Retigabine/Phenoxybenzamine**	**302,1317**	**C18H22ClNO**	**1**
317,1441	**NA**	**[M-H]-**	**Imidazolone A**	**317,1467**	**C12H22N4O6**	**8**
327,2301	327,2306	[M-H]-	Docosahexaenoic acid	327,233	C22H32O2	7
346,0498	346,0533	[M-H]-	AMP	346,0558	C10H14N5O7P	17
362,0446	362,0482	[M-H]-	GMP	362,0507	C10H14N5O8P	7
392,1459	**392,1469**	**[M-H]-**	**gamma-Glutamylfelinylglycine**	**392,1497**	**C15H27N3O7S**	**7**
404,0078	404,0094	[M+Cl]-	Thioflosulide	403,9999	C16H13F2NO3S2	24
435,1134	**435,1165**	**[M-H]-**	**Bis-(1,3-diethylthiobarbituric acid)trimethine oxonol**	**435,1166**	**C19H24N4O4S2**	**0**

Supplemental Table 1. List of significantly different metabolites in mouse kidney samples assigned by the mass measurements using both MALDI-TOF/TOF and MALDI-FTICR MS in negative ion mode. *(continued)*

calibrated m/z from MALDI-TOF/TOF	m/z from MALDI-FTICR	Ion	Annotation*	Theoretical m/z	Formula	ppm
465,3012	465,3015	[M-H]-	LPA(20:0)	465,2987	C23H47O7P	5
525,2793	**525,2824**	**[M-H]-**	**LPE(22:6)****	**525,2817**	**C27H44NO7P**	**1**
552,2737	**552,2707**	**[M-H]-**	**Vignatic acid A**	**552,2715**	**C30H39N3O7**	**1**
579,0235	579,0249	[M-H]-	UDP-GlcUA	579,027	C15H22N2O18P2	4
721,5017	721,4737	[M-H]-	PA(38:5)	721,4814	C41H71O8P	11
737,5024	NA	[M-H]-	SM(d16:1/20:3(5Z,11Z,14Z)-O(8,9))/SM(d16:1/20:4(6E,8Z,11Z,14Z)-OH(5S))	737,5239	C41H75N2O7P	12
747,5204	747,5197	[M-H]-	PG(34:1)	747,5182	C40H77O10P	2
833,5226	**833,5206**	**[M-H]-**	**PI(34:2)**	**833,5186**	**C43H79O13P**	**2**
834,5216	834,5285	[M-H]-	PS(40:6)	834,5291	C46H78NO10P	1
835,535	835,5298	[M-H]-	PI(34:1)	835,5342	C43H81O13P	5
838,5605	838,5572	[M-H]-	PS(40:4)	838,5604	C46H82NO10P	4
857,5194	**857,5165**	**[M-H]-**	**PI(36:4)**	**857,5186**	**C45H79O13P**	**2**
909,5529	909,553	[M-H]-	PI(40:6)	909,5499	C49H83O13P	3
882,5253	**882,5216**	**[M-H]-**	**PS(44:10)**	**882,5291**	**C50H78NO10P**	**8**

* only one representative lipid name was shown for some m/z features

** lipid isotope

§ Breakdown product of protein catabolism

Not a natural metabolite, part of exposome

Bold; metabolites in diabetes and FMD groups are both significantly different from control

Supplemental Table 2. Measurements of significantly different metabolites in mouse kidney sample

Calibrated m/z from MALDI-TOF/TOF	Peak intensity control (A.U.)						Peak intensity diabetes (A.U.)						Peak intensity FMD (A.U.)					
	1	2	3	4	mean	stdev	1	2	3	4	mean	stdev	1	2	3	4	mean	stdev
193,02	1,679	2,015	2,524	1,809	2,007	0,372	6,114	1,528	3,239	2,018	3,225	2,056	3,235	3,105	2,914	2,592	2,961	0,279
203,07	2,132	3,419	1,895	2,939	2,596	0,708	1,198	1,030	1,091	1,048	1,092	0,076	0,972	1,128	1,179	1,202	1,120	0,104
241,06	4,045	3,296	2,023	2,286	2,912	0,934	1,629	1,944	1,845	1,829	1,812	0,132	1,235	1,322	1,555	1,373	1,371	0,135
245,11	1,090	1,016	0,810	1,202	1,029	0,165	0,639	0,707	0,633	0,670	0,662	0,034	0,462	0,613	0,683	0,552	0,577	0,094
249,05	2,277	3,097	2,399	3,222	2,749	0,480	1,681	1,299	1,360	1,343	1,420	0,175	1,242	1,475	1,580	1,263	1,390	0,165
273,09	0,946	0,841	1,082	0,929	0,949	0,100	1,058	1,232	1,444	1,667	1,350	0,264	0,936	1,152	1,164	0,953	1,051	0,124
275,09	9,283	10,564	9,445	11,023	10,079	0,849	5,692	5,557	6,655	5,537	5,860	0,534	4,806	6,076	7,033	5,583	5,874	0,933
279,04	0,844	0,891	0,761	0,752	0,812	0,067	0,685	0,556	0,676	0,668	0,646	0,061	0,685	0,703	0,717	0,642	0,687	0,033
288,12	0,692	0,745	0,572	0,821	0,708	0,105	0,472	0,398	0,542	0,531	0,486	0,066	0,445	0,480	0,559	0,421	0,476	0,060
302,13	0,929	1,085	0,923	1,096	1,008	0,095	0,726	0,870	0,718	0,736	0,763	0,072	0,508	0,762	0,763	0,617	0,662	0,124
317,14	0,888	0,963	0,805	1,030	0,922	0,097	0,638	0,614	0,626	0,682	0,640	0,030	0,478	0,584	0,697	0,553	0,578	0,091
327,23	0,823	0,741	0,654	0,622	0,710	0,091	0,552	0,702	0,587	0,488	0,582	0,090	0,485	0,488	0,600	0,449	0,505	0,066
346,05	32,576	34,299	24,874	28,267	30,004	4,258	21,570	30,909	20,466	25,398	24,586	4,716	13,517	20,229	15,993	19,903	17,410	3,231
362,04	2,122	2,347	1,849	1,921	2,060	0,224	1,569	2,128	1,830	1,687	1,804	0,241	1,428	1,457	1,364	1,714	1,491	0,154
392,15	0,634	0,641	0,569	0,602	0,611	0,033	0,445	0,414	0,521	0,506	0,472	0,050	0,438	0,478	0,564	0,416	0,474	0,065
404,01	2,344	2,145	1,638	2,093	2,055	0,299	1,299	2,309	1,499	1,602	1,677	0,439	0,857	1,276	1,290	1,568	1,248	0,293
435,11	4,288	4,357	4,086	3,574	4,076	0,354	2,640	3,248	3,380	3,207	3,119	0,327	2,460	2,997	2,517	1,850	2,456	0,471
465,30	1,946	2,057	2,147	1,424	1,894	0,323	2,245	2,242	2,773	2,123	2,346	0,290	2,896	3,025	2,423	2,366	2,677	0,332
525,28	5,464	5,256	5,335	4,847	5,226	0,267	4,844	4,647	4,726	4,260	4,619	0,253	3,923	3,808	4,821	3,671	4,056	0,521
552,27	11,836	11,578	12,412	11,374	11,800	0,450	9,897	10,121	8,729	9,294	9,510	0,627	6,765	7,066	9,486	8,509	7,957	1,272
579,02	0,420	0,446	0,470	0,478	0,453	0,026	0,333	0,345	0,395	0,409	0,371	0,037	0,340	0,380	0,454	0,324	0,375	0,058
721,50	0,814	0,790	0,830	0,814	0,812	0,016	0,753	0,652	0,723	0,679	0,702	0,045	0,699	0,651	0,825	0,687	0,716	0,076
737,50	0,702	0,744	0,748	0,708	0,726	0,024	0,834	0,762	0,891	0,800	0,821	0,055	0,800	0,784	0,857	0,832	0,819	0,033
747,52	4,855	4,402	4,679	5,198	4,783	0,333	3,874	4,209	3,819	3,646	3,887	0,236	3,556	2,928	4,662	4,831	3,994	0,908
833,52	2,075	2,181	1,940	1,787	1,996	0,171	1,650	1,613	1,559	1,478	1,575	0,074	1,537	1,239	1,511	1,700	1,497	0,191
834,52	5,732	5,874	6,343	4,578	5,632	0,749	5,199	5,209	5,183	4,825	5,104	0,187	4,288	3,914	4,606	4,472	4,320	0,301
835,54	3,669	3,726	4,253	2,946	3,649	0,537	3,286	3,344	3,315	3,017	3,240	0,151	2,792	2,535	2,937	2,952	2,804	0,193
838,56	5,012	6,482	7,568	3,916	5,744	1,607	6,564	6,103	6,872	6,131	6,417	0,369	5,691	5,602	5,491	5,165	5,487	0,230
857,52	5,157	5,341	4,819	4,395	4,928	0,416	4,073	4,181	4,342	3,671	4,067	0,286	3,689	3,225	4,006	4,034	3,738	0,376
909,55	2,819	2,170	1,886	1,871	2,186	0,443	1,840	1,869	1,341	1,198	1,562	0,343	1,217	1,031	1,521	1,242	1,253	0,202
882,53	0,944	0,836	0,799	0,764	0,836	0,078	0,713	0,720	0,665	0,618	0,679	0,048	0,606	0,574	0,755	0,642	0,644	0,079

Bold metabolites in diabetes and FMD groups are both significantly different from control